PHYSICAL REVIEW B **80**, 041404(R) (2009)

Coulomb versus spin-orbit interaction in few-electron carbon-nanotube quantum dots

Andrea Secchi[1,2] and Massimo Rontani[1,*]
[1]*CNR–INFM National Research Center S3, Via Campi 213/A, 41125 Modena, Italy*
[2]*Dipartimento di Fisica, Università degli Studi di Modena e Reggio Emilia, Via Campi 213/A, 41125 Modena, Italy*
(Received 29 March 2009; revised manuscript received 24 June 2009; published 16 July 2009)

Few-electron states in carbon-nanotube quantum dots are studied by means of the configuration-interaction method. The peculiar noninteracting feature of the tunneling spectrum for two electrons, recently measured by F. Kuemmeth, S. Ilani, D. C. Ralph, and P. L. McEuen [Nature (London) **452**, 448 (2008)], is explained by the splitting of a low-lying isospin multiplet due to spin-orbit interaction. Nevertheless, the strongly interacting ground state forms a "Wigner molecule" made of electrons localized in space. Signatures of the electron molecule may be seen in tunneling spectra by varying the tunable dot confinement potential.

DOI: 10.1103/PhysRevB.80.041404 PACS number(s): 73.63.Fg, 73.20.Qt, 73.22.Lp, 73.23.Hk

After almost two decades of research, carbon nanotubes (CNs) (Ref. 1) still provide a venue for the investigation of fundamental properties of interacting electron systems, such as Luttinger-liquid[2] and Wigner-crystal[3] behaviors, Mott state,[4] Kondo effect,[5] and Andreev transport[6] in CN quantum dots (QDs). With respect to semiconductor QDs,[7,8] low-screening, ultraclean CN QDs appear to be ideal candidates[3] for the realization of long-sought "Wigner molecules" (WMs) (Ref. 8) of strongly correlated electrons. These classical geometrical configurations of electrons localized in space are insensitive to the spin state of the system.[3,8] On the other hand, recently Kuemmeth *et al.*[9] showed that orbital and spin degrees of freedom are entangled by strong spin-orbit interaction in single-wall CN QDs, disproving the popular shell model based on the fourfold degeneracy of QD energy levels.[10,11] Intriguingly, the two-electron tunneling spectrum measured in Ref. 9 was well explained by a noninteracting model with spin-orbit coupling. So far, it is unclear if the WM state[8] may survive to the perturbation induced by spin-orbit interaction.

In this Rapid Communication we show that noninteracting features of the tunneling spectrum, due to spin-orbit coupling, coexist with the strongly interacting nature of few-electron states, as seen from configuration interaction (CI, also known as exact diagonalization) calculations. Electrons in realistic dots form one-dimensional WMs, which may already have been observed in experiments.[3,9] We predict that molecular signatures appear in the excitation spectrum by varying the QD confinement potential.

We focus on a QD embedded in a semiconducting CN whose length scale, ℓ_{QD}, is smaller that the CN length. Hence, ℓ_{QD} is the relevant single-particle (SP) length and the effects of the CN boundaries may be neglected. With respect to previous calculations,[11–14] we assume the QD to be defined by an external gate potential, slowly varying on the lattice scale, which we model as a one-dimensional harmonic oscillator (HO) of frequency ω_0. The quadratic potential is the low-energy generic form for a soft confinement,[15] setting $\ell_{\mathrm{QD}}=(\hbar/m^*\omega_0)^{1/2}$, where $m^*=\hbar^2/3R\gamma$ is the effective mass, R is the CN radius, and $\gamma=0.54$ eV·nm is the graphene π-band parameter. SP states $\psi_{n\tau_z}(\boldsymbol{r})=\mathcal{N}F_n(x)\phi_{\tau_z}(\boldsymbol{r})$ are obtained by the envelope-function modulation $F_n(x)$ of bulk states $\phi_{\tau_z}(\boldsymbol{r})$ at the two nonequivalent minima of the lowest conduction band. The isospin index $\tau_z=+1$ (-1) labels valley K (K'), $F_n(x)$ is the wave function of the nth HO excited state, and $\mathcal{N}$ is a normalization factor. Here $\phi_{\tau_z}(\boldsymbol{r})=\exp(-iy\tau_z/3R)[\psi_{X,A}(\boldsymbol{r})+\tau_z\psi_{X,B}(\boldsymbol{r})]$, where $\psi_{X,A}(\boldsymbol{r})$ and $\psi_{X,B}(\boldsymbol{r})$ are the Bloch tight-binding states for sublattices A and B, respectively, at point $X=K$ $(X=K')$ in the reciprocal space for $\tau_z=+1$ (-1). The isospin $\tau_z=+1$ (-1) points to the (anti)clockwise rotation along the circumference coordinate y, perpendicular to the tube axis x. The interacting Hamiltonian is $\hat{H}=\hat{H}_{\mathrm{SP}}+\hat{V}_{\mathrm{FW}}+\hat{V}_{\mathrm{BW}}$, which includes the SP term $\hat{H}_{\mathrm{SP}}=\sum_{n\tau_z\sigma_z}\varepsilon_{n\tau_z\sigma_z}\hat{c}^\dagger_{n\tau_z\sigma_z}\hat{c}_{n\tau_z\sigma_z}$, as well as the two-body terms for forward (FW) and backward (BW) Coulomb scattering processes $\hat{V}_{\mathrm{FW}}$ and $\hat{V}_{\mathrm{BW}}$, respectively.[12,14,16] Here $\hat{c}_{n\tau_z\sigma_z}$ destroys an electron occupying the SP orbital $\psi_{n\tau_z}(\boldsymbol{r})$ with spin σ_z. The SP energy $\varepsilon_{n\tau_z\sigma_z}$ includes the dominant term of spin-orbit interaction due to the CN curvature[9,17,18] as well as the contribution of an axial magnetic field B,[17]

$$\varepsilon_{n\tau_z\sigma_z}=\varepsilon_n^{\mathrm{HO}}+\Delta_{\mathrm{SO}}\frac{\gamma}{R}\tau_z\sigma_z+\mu_{\mathrm{B}}B\left(\frac{g^*}{2}\sigma_z-\frac{mR\gamma}{\hbar^2}\tau_z\right). \quad (1)$$

Here $\varepsilon_n^{\mathrm{HO}}=\gamma/3R+\hbar\omega_0(n+1/2)$, Δ_{SO} is the spin-orbit coupling term, μ_{B} is the Bohr magneton, and g^* is the giromagnetic factor. The two-body terms $\hat{V}_{\mathrm{FW}}$ and $\hat{V}_{\mathrm{BW}}$ are of the type $\hat{V}=1/2\sum V_{\alpha\beta\gamma\delta}\hat{c}^\dagger_{\alpha\sigma_z}\hat{c}^\dagger_{\beta\sigma'_z}\hat{c}_{\gamma\sigma'_z}\hat{c}_{\delta\sigma_z}$, where $\alpha\equiv(n,\tau_z)$ and $V_{\alpha\beta\gamma\delta}$ is the matrix element of the Ohno potential $V(\boldsymbol{r}-\boldsymbol{r}')=U_0(1+\epsilon^2|\boldsymbol{r}-\boldsymbol{r}'|^2U_0^2/e^4)^{-1/2}$, which interpolates the two limits of Coulomb-like long-range and Hubbard-like short-range interactions (ϵ is the relative dielectric constant, and $U_0=15$ eV).[14] In the envelope function approach[19] the underlying graphene physics is buried into the precise form of $V_{\alpha\beta\gamma\delta}$'s, which depend on both Bloch states $\phi_{\tau_z}(\boldsymbol{r})$ and envelopes $F_n(x)$. We evaluate $V_{\alpha\beta\gamma\delta}$ by considering explicitly the tight-binding expansion of $\phi_{\tau_z}(\boldsymbol{r})$ (cf. Ref. 14). FW and BW terms correspond to direct $[(\tau_z,\tau'_z)\to(\tau_z,\tau'_z)]$ and exchange $[(\tau_z,\tau'_z)\to(\tau'_z,\tau_z)$ and $\tau_z\neq\tau'_z]$ isospin scattering processes, respectively.[12,14,16]

The few-body problem is solved by means of the CI method.[8,20] We diagonalize $\hat{H}$, which is a matrix in the basis of the Slater determinants $|\Phi_i\rangle$ obtained by filling with N electrons in all possible ways the thirty lowest-energy SP

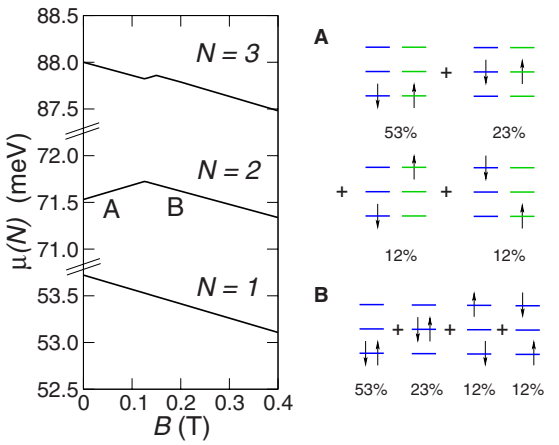

FIG. 1. (Color online) Left: $\mu(N)$ vs B for $1 \leq N \leq 3$. Right: main configurations contributing to states A and B. Blue [dark gray] (green [light gray]) levels are HO states with isospin $\tau_z=+1$ (-1), whereas up (down) arrows stand for electron spin $\sigma_z=+1$ (-1). The percentages are the weights of the Slater determinants in the CI expansion of the wave function.

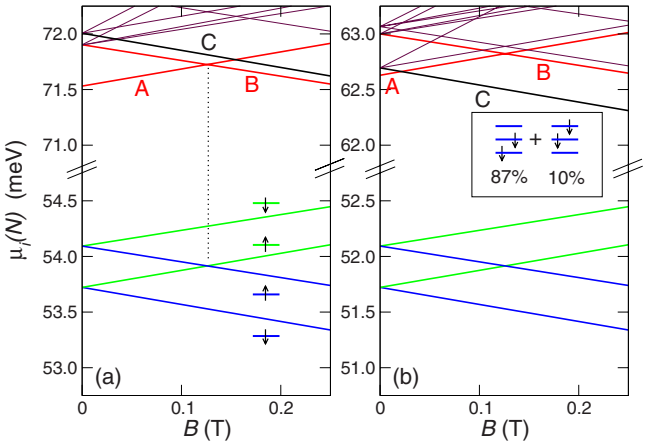

FIG. 2. (Color online) $\mu_i(N)$ vs B for $N=1,2$, for (a) $\hbar\omega_0=8$ meV, and for (b) $\hbar\omega_0=4$ meV. Inset: main configurations in the CI expansion of the wave function of state C.

orbitals $\psi_\alpha(\boldsymbol{r})$. We obtain energies and wave functions of the many-body ground and excited states $|\Psi^{(n)}\rangle$, written as linear combinations of $|\Phi_i\rangle$'s, $|\Psi^{(n)}\rangle=\Sigma c_i^{(n)}|\Phi_i\rangle$, in each sector of the Fock space labeled by N, the z component of the total spin S_z, and the total parity under spatial inversion $x \to -x$.

To compare with tunneling spectra,[9] we compute the chemical potential $\mu(N)$ for a given value of B, $\mu_{(i)}(N)=E_{0(i)}(N)-E_0(N-1)$, where $E_0(N)$ $(E_i(N))$ is the energy of the many-body ground (ith excited) state with N electrons. The predicted $\mu(N)$'s may be converted into the gate voltages at which electrons tunnel into the QD.[8] We infer from Ref. 9 the inputs of CI calculation, i.e., $\hbar\omega_0=8$ meV, $R=3.6$ nm, $\Delta_{\mathrm{SO}}=1.24\cdot10^{-3}$, and $g^*=2.14$. The unknown value of ϵ is a fit parameter for a small-gap semiconductor, which may be strongly affected by the leads. By choosing $\epsilon=3.5$ we obtain the curves of Fig. 1, $\mu(N)$ vs B for $1 \leq N \leq 3$, which compare well with those of Fig. (3a) in Ref. 9. The plot quantitatively reproduces the dependence of $\mu(N)$ on B, specifically the kink of $\mu(2)$ at $B_c \approx 0.125$ T and $\mu(3)$ at ≈ 0.15 T.[21] As a check of consistency with the experiment, we remark that the CI spacing between $\mu(2)$ and $\mu(1)$ at $B=0$, 17.8 meV, agrees within 6% with the value estimated in Ref. 9.

The kink of $\mu(2)$ at B_c is due to the crossing between different ground states of two electrons, labeled A (B) for $B<B_c$ $(B>B_c)$ (cf. Fig. 1). To gain insight into their nature, let us briefly consider also excited-state contributions to $\mu_i(N)$, which are shown in Fig. 2(a) for $N=1,2$. Note that Fig. 2(a) perfectly matches Fig. (3c) of Ref. 9. The four lowest-energy SP levels $\mu_i(1)$ are explicitly shown. Blue [dark gray] (green [light gray]) lines indicate states with $\tau_z=1$ (-1), whose orbital magnetic moment is (anti)parallel to the CN axis, decreasing (increasing) its energy with B. The fourfold degeneracy of the levels ($\tau_z=\pm1$ and $\sigma_z=\pm1$) at $B=0$ is split by spin-orbit interaction, which entangles orbital and spin degrees of freedom.[9] This induces an isospin transition $(\tau_z=-1 \to \tau_z=1)$ for the first excited noninteracting level $\mu_1(1)$ at $B \approx 0.125$ T. Remarkably, this field is exactly the *same* as the critical value B_c at which the A $\to$ B transition occurs [cf. the vertical dashed line in Fig. 2(a)]. Because of this feature, it was argued in Ref. 9 that the A $\to$ B transition may be solely explained in terms of spin-orbit interaction. State A was supposed to be a single Slater determinant with the electrons in the two lowest spin-orbitals, ($\tau_z=1$ and $\sigma_z=-1$) and ($\tau_z=-1, \sigma_z=1$), whereas B is obtained by moving the electron from ($\tau_z=-1, \sigma_z=1$) to ($\tau_z=1, \sigma_z=1$). In this picture correlation effects are absent. We next show that A and B are instead strongly interacting states.

The right panel of Fig. 1 shows the Slater determinants with the largest weights in the CI expansion of $|A\rangle$. The blue [dark gray] (green [light gray]) ladders of levels depict the HO states for $\tau_z=+1$ (-1), whereas arrows represent spins. The main configuration, whose weight is 53%, is the Slater determinant proposed in Ref. 9 for the ground state. However, CI calculation shows that there are other three relevant determinants where also the excited states of the HO are populated (Fig. 1). This is due to the correlated character of $|A\rangle$: the strongest the impact of Coulomb interaction, the largest the mixing of determinants. Similarly, state B shown in the right panel of Fig. 1 is correlated as well. Besides, state B may be obtained from A by replacing the levels with $\tau_z=-1$ with those with $\tau_z=1$ (Fig. 1). Hence, A and B belong to a *isospin multiplet*, only differing in the projections T_z of the isospin. Here the isospin vector is defined by $\hat{\boldsymbol{T}}=2^{-1}\Sigma_{n\tau_z\tau_z'\sigma_z}\hat{c}^\dagger_{n\tau_z\sigma_z}\boldsymbol{\sigma}_{\tau_z\tau_z'}\hat{c}_{n\tau_z'\sigma_z}$, where the components of $\boldsymbol{\sigma}$ are the Pauli matrices [e.g., $\hat{T}_z=(\hat{n}_{+1}-\hat{n}_{-1})/2$ with $\hat{n}_{\tau_z}=\Sigma_{n\sigma_z}\hat{c}^\dagger_{n\tau_z\sigma_z}\hat{c}_{n\tau_z\sigma_z}$]. This is confirmed by extrapolating the behavior of A and B to the limit $\Delta_{\mathrm{SO}} \to 0$ (not shown). In this limit, A and B and other states at higher energies collapse into a sixfold multiplet, which includes three spin triplet ($T=0$, $S=1$, and $S_z=\pm1,0$) plus three isospin triplet ($S=0$, $T=1$, and $T_z=\pm1,0$) states. In fact, the total wave functions must be odd, whereas their (unique) orbital part is even under particle exchange. Therefore, except for a tiny residual splitting of ≈ 2 μeV due to BW interaction, the A-B energy separation depends on spin-orbit interaction only.

From Eq. (1) and the inspection of CI wave functions of Fig. 1, it is clear that the energy splitting between A and B at

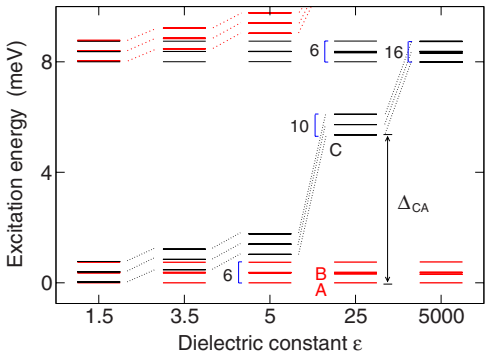

FIG. 3. (Color online) Two-electron excitation energies vs ϵ, reckoned from the ground state. Red [light gray] (black [dark gray]) lines correspond to even (odd) parity states.

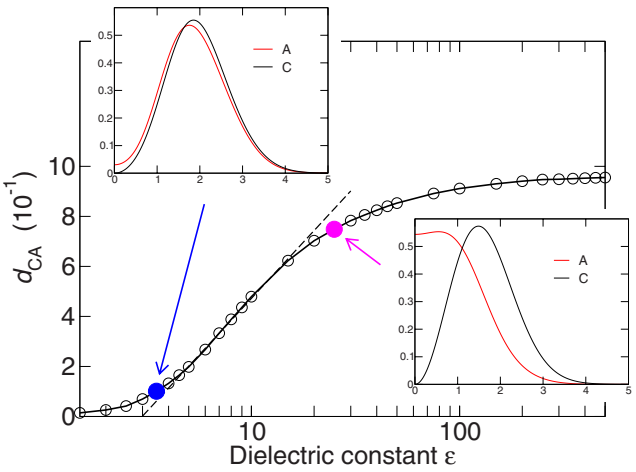

FIG. 4. (Color online) d_{CA} vs ϵ. The dashed line is a linear fit to data in the range $5 \leq \epsilon \leq 15$ with correlation coefficient 0.999. Insets: $g_A(x)$ and $g_C(x)$ vs x, for $\epsilon=3.5$ (top left) and 25 (bottom right). The length unit is ℓ_{QD}.

zero field, $\mu_1(2)-\mu(2)=2\Delta_{SO}\gamma/R$, is the same as that between one-electron levels, $\mu_1(1)-\mu(1)$ [cf. Fig. 2(a)]. Besides, $\mu(N)$ depends on B through the spin and orbital magnetic dipole moments [cf. Eq. (1)], which are linear in $\Delta S_z = S_z(N)-S_z(N-1)$ and $\Delta T_z = T_z(N)-T_z(N-1)$, respectively. It is immediate to verify that ΔS_z and ΔT_z are the same for both $\mu(2)$ and $\mu_1(1)$, for $B<B_c$ ($\Delta S_z=1/2$ and $\Delta T_z=-1/2$) and $B>B_c$ ($\Delta S_z=1/2$ and $\Delta T_z=1/2$). This explains why the critical value of the field for both $\mu(2)$ and $\mu_1(1)$ is the same despite the correlated nature of A and B, in agreement with the key experimental observation of Ref. 9.

The noninteracting feature of $\mu(2)$ discussed above is *not* universal and may be affected by electron correlation. This is the case as one changes, e.g., the QD potential, which is controlled in the laboratory by a capacitively coupled gate. This in turn changes the ratio of Coulomb matrix elements V to the SP spacing $\hbar\omega_0$. Figure 2(b) shows the analogous plot of Fig. 2(a) for half the value of the confinement energy, $\hbar\omega_0=4$ meV. The pattern of $\mu(2)$ vs B has now changed with respect to Fig. 2(a), due to the crossing between A and a new state, labeled C in the plot, occurring close to the origin, at $B\approx 0.02$ T. This critical value depends on the splitting Δ_{CA} between C and A at zero field, which in turn is sensitive to Coulomb correlation. A similar result has been recently reported by Wunsch for a square-well QD.[22]

The crucial role of Coulomb interaction in the QD is fully appreciated by considering the excitation spectrum. Figure 3 shows the two-electron excitation spectrum vs the dielectric constant ϵ, which affects the relevance of correlation effects. The lower bound on the horizontal axis ($\epsilon=1.5$) mimics low screening, typical of large-gap semiconducting CNs, whereas the upper bound ($\epsilon=5000$) may be regarded as the noninteracting limit. In the latter, all levels bunch into the HO levels, uniformly spaced by $\hbar\omega_0$ (=8 meV). In the lowest set of levels (red [light gray] lines) the two electrons occupy the nodeless orbitals in one of the two valleys, whereas the next set (black [dark gray] lines) is obtained by promoting one electron into the first HO excited state. The states of the first (second) set have even (odd) parity. Within each set, a residual fine structure survives, entirely due to spin-orbit interaction. As indicated in Fig. 3, the total number of levels in the first (second) set is 6 (16), given by the possible ways to arrange the two electrons either in the same or in different valleys compatibly with Pauli's exclusion principle.

As ϵ is reduced in Fig. 3, Coulomb interaction alters the energy spectrum. In fact, the sixteen odd levels belonging to the second set separate into two multiplets. A first sixfold multiplet is insensitive to ϵ, whereas a second tenfold multiplet experiences a sudden energy drop. The former multiplet is associated to the collective motion of the center of mass (Kohn mode), which is decoupled from the relative motion and hence unaffected by Coulomb interaction.[8] The sixfold degeneracy of this odd multiplet, lifted only by spin-orbit interaction, is the same as that of the lowest even multiplet since they differ only in the excitation of the center of mass coordinate. The second odd multiplet is instead sensitive to ϵ, i.e., Coulomb interaction. In fact, Δ_{CA} becomes a small fraction of $\hbar\omega_0$ at the experimental value of $\epsilon=3.5$ ($\Delta_{CA}/\hbar\omega_0\approx 0.06$), whereas it vanishes at $\epsilon=1.5$. As discussed below, such vanishing points to the formation of a WM, the state where Coulomb correlation localizes electrons in space to minimize their electrostatic energy.[3,8]

The insets of Fig. 4 show the correlation function $g(x)$ vs x for states A and C. $g(x)$ is the probability of finding the two electrons at relative distance $x=x_1-x_2$ [normalized as $\int_0^\infty g(x)dx=1$, with $g(x)=g(-x)$]. As ϵ decreases from $\epsilon=25$ (bottom right inset) to the experimental value $\epsilon=3.5$ (top left inset), the ground-state probability distribution $g_A(x)$ (red [light gray] curve) develops a well-defined peak at $x_0=1.7$, showing that electrons localize in space and freeze their mutual distance. x_0 compares well with the equilibrium value $x_{0,cl}=1.6$ of two pointlike *classical* particles in the HO trap interacting via the Coulomb potential $e^2/\epsilon|x|$. Note that crystallization proceeds by removing probability weight from g_A at the origin. As localization is fully accomplished, $g_A(x=0)\to 0$, which is compatible with both even and odd states such as A and C, respectively. In fact, $g_A(x)$ (red [light gray] curve) and $g_C(x)$ (black [dark gray] curve) tend to coincide as well as $\Delta_{CA}\to 0$ as ϵ decreases (cf. Fig. 3). Similarly, as the overlap between the probability weights of localized electrons is suppressed, exchange interaction is

negligible and different values of S_z ($S_z=0$ for A and $S_z=-1$ for C) are admissible. In this limit states A and C, which only differ for now irrelevant quantum numbers like parity and spin, represent the same "classical" configuration.

We exploit the progressive overlap between $g_A(x)$ and $g_C(x)$ as ϵ is reduced to characterize the transition to the WM state. In Fig. 4 we plot vs ϵ the functional distance d_{CA} between states A and C, defined as $d_{CA}=\int_0^\infty dx|g_A(x)-g_C(x)|$. The semilog plot allows to identify three separate regions, where d_{CA} scales differently with ϵ (there are no sharp transitions in finite-size systems). For $\epsilon>20$, d_{CA} slowly tends to the upper bound 1 since the location of the maximum of $g_A(x)$ approaches the origin whereas $g_C(x)$ has a node there. The large probability of finding two particles close to each other ($x\approx 0$) highlights the absence of a correlation hole in the ground state (cf. the magenta [light gray] dot and related plot). In the crossover region, $5<\epsilon<20$, $d_{CA}\propto \log \epsilon$ as shown by the linear fit in Fig. 4 (dashed line). Here a significant correlation hole rapidly forms in A as ϵ decreases. The WM corresponds to $\epsilon<5$, where $d_{CA}<0.1$ and it slowly decreases with ϵ, as $g_A(x)$ and $g_C(x)$ overlap almost perfectly. Remarkably, the observed case[9] of $\epsilon=3.5$ (blue [dark gray] dot in Fig. 4) occurs in this region.

The squeezing of the QD confinement potential via an external gate is a handle to drive Wigner crystallization, since the effect of lowering $\hbar\omega_0$ [Fig. 2(b)] is similar to that of decreasing ϵ (Figs. 3 and 4). In fact, the critical B value of the A$\rightarrow$C transition reported in Fig. 2(b) is a measure of the vanishing of Δ_{CA}. As $\hbar\omega_0$ is reduced, this critical field approaches zero, implying that the spin-polarized phase C may be induced with no energy cost. The latter behavior has been observed for hole WMs.[3]

We have shown that spin-orbit and strong Coulomb interaction coexist in CN QDs, leading to the formation of WMs at experimentally attainable regimes. This insight into the entangled orbital and spin degrees of freedom is relevant for the all-electrical[9] and all-optical[23] manipulation of electron spins in CN-based devices.

We thank F. Manghi, E. Molinari, E. Andrei, and G. Steele for stimulating discussions. This work is supported by INFM-CINECA Supercomputing Project 2008–2009.

*Website and email addresses: www.nanoscience.unimore.it/max_html; rotani@unimore.it

[1] R. Saito, G. Dresselhaus, and M. S. Dresselhaus, *Physical Properties of Carbon Nanotubes* (Imperial College Press, London, 1998).

[2] M. Bockrath, D. H. Cobden, J. Lu, A. G. Rinzler, R. E. Smalley, L. Balents, and P. L. McEuen, Nature (London) **397**, 598 (1999).

[3] V. V. Deshpande and M. Bockrath, Nat. Phys. **4**, 314 (2008).

[4] V. V. Deshpande, B. Chandra, R. Caldwell, D. S. Novikov, J. Hone, and M. Bockrath, Science **323**, 106 (2009).

[5] J. Nygård, D. H. Cobden, and P. E. Lindelof, Nature (London) **408**, 342 (2000).

[6] J. A. van Dam, Y. V. Nazarov, E. P. A. M. Bakkers, S. De Franceschi, and L. P. Kouwenhoven, Nature (London) **442**, 667 (2006).

[7] S. Kalliakos, M. Rontani, V. Pellegrini, C. P. García, A. Pinczuk, G. Goldoni, E. Molinari, L. N. Pfeiffer, and K. W. West, Nat. Phys. **4**, 467 (2008).

[8] S. M. Reimann and M. Manninen, Rev. Mod. Phys. **74**, 1283 (2002).

[9] F. Kuemmeth, S. Ilani, D. C. Ralph, and P. L. McEuen, Nature (London) **452**, 448 (2008).

[10] W. Liang, M. Bockrath, and H. Park, Phys. Rev. Lett. **88**, 126801 (2002); D. H. Cobden and J. Nygård, *ibid.* **89**, 046803 (2002); P. Jarillo-Herrero, J. Kong, H. S. J. van der Zant, C. Dekker, L. P. Kouwenhoven, and S. De Franceschi, *ibid.* **94**, 156802 (2005); S. Moriyama, T. Fuse, M. Suzuki, Y. Aoyagi, and K. Ishibashi, *ibid.* **94**, 186806 (2005).

[11] Y. Oreg, K. Byczuk, and B. I. Halperin, Phys. Rev. Lett. **85**, 365 (2000).

[12] R. Egger and A. O. Gogolin, Phys. Rev. Lett. **79**, 5082 (1997); Eur. Phys. J. B **3**, 281 (1998).

[13] D. V. Bulaev, B. Trauzettel, and D. Loss, Phys. Rev. B **77**, 235301 (2008).

[14] L. Mayrhofer and M. Grifoni, Eur. Phys. J. B **63**, 43 (2008).

[15] See, e.g., A. Kumar, S. E. Laux, and F. Stern, Phys. Rev. B **42**, 5166 (1990).

[16] T. Ando, J. Phys. Soc. Jpn. **75**, 024707 (2006).

[17] T. Ando, J. Phys. Soc. Jpn. **69**, 1757 (2000).

[18] D. Huertas-Hernando, F. Guinea, and A. Brataas, Phys. Rev. B **74**, 155426 (2006).

[19] J. M. Luttinger and W. Kohn, Phys. Rev. **97**, 869 (1955).

[20] M. Rontani, C. Cavazzoni, D. Bellucci, and G. Goldoni, J. Chem. Phys. **124**, 124102 (2006).

[21] The energy conversions of Figs. 2(c) and 3(a) in Ref. 9 are inconsistent. We take the voltage-to-energy ratio of Fig. 2(c) as a reference.

[22] B. Wunsch, Phys. Rev. B **79**, 235408 (2009).

[23] C. Galland and A. Imamoğlu, Phys. Rev. Lett. **101**, 157404 (2008).